ELSEVIER

Journal of Alloys and Compounds 286 (1999) 203–207

Journal of ALLOYS AND COMPOUNDS

X-ray powder diffraction study of cation distribution and the $Fd3m \rightarrow P4_132$ symmetry reduction in $Li_{0.5}Fe_{2.5}O_4/LiMn_2O_4$ spinel solid solutions

E. Wolska[a,*], P. Piszora[a], K. Stempin[a], C.R.A. Catlow[b]

[a]*Adam Mickiewicz University, Faculty of Chemistry, Department of Magnetochemistry, ul.Grunwaldzka 6, PL-60780 Poznań, Poland*
[b]*The Royal Institution of Great Britain, Davy–Faraday Research Laboratory, 21 Albemarle St., London W1X 4BS, UK*

Abstract

Structural changes in solid solutions formed between the cubic normal spinel, $LiMn_2O_4$, and ordered inverse spinel, $Li_{0.5}Fe_{2.5}O_4$, have been investigated by X-ray powder diffraction and infrared spectroscopic techniques.

By refining the X-ray diffraction patterns with Rietveld profile analysis, the lattice parameters, interatomic distances and cation distribution were determined. The Fe-for-Mn substitution increases the spinel unit-cell constant from 8.21Å to 8.34Å for the Fe/(Fe+Mn) mole ratio of 0 and 1, respectively. A distinct departure from Vegard's law appears for Fe/(Fe+Mn)≥0.6. The additional 'superstructure' reflections on the X-ray patterns confirm an ordering of lithium ions in octahedral sites, bringing about the lowering of *Fd*3*m* symmetry to the $P4_132/P4_332$ space group. Li^+ ions are distributed over both octahedral and tetrahedral cationic positions of spinel lattice, although the end-members of the solid solution series, $LiMn_2O_4$ and $Li_{0.5}Fe_{2.5}O_4$, contain Li^+ coordinated tetrahedrally and octahedrally, respectively.

The ordering of Li^+ ions in the 4*b* Wyckoff's positions of a cubic primitive unit cell ($P4_132/P4_332$), observed for the increasing Fe^{3+} content, has been confirmed for that system with infrared spectroscopy. The number of infrared active vibrations increases significantly with the lowering of crystal symmetry caused by the 1:3 ordering of Li^+ in octahedral sites.

Keywords: Spinel-type metal oxides; $LiMn_2O_4$; $LiFe_5O_8$; Lithium ions in spinel structures; Lithium–iron–manganese oxides; Lithium ferrite; Rietveld refinement; Infrared spectroscopy

1. Introduction

Investigations on the lithium ion distribution in the spinel-type lithium–iron–manganese oxides have been carried out on the very limited ranges of $LiMn_2O_4$/$LiFe_5O_8$ solid solutions. Stoichiometric cubic spinel $LiMn_2O_4$ has the Li^+ ions occupying the tetrahedral 8*a* sites, and a 1:1 mixture of Mn^{3+} and Mn^{4+} ions randomly distributed over the octahedral 16*d* positions in the spinel lattice (space group *Fd*3*m*). Lithium ferrite, in both disordered and order forms, displays an inverse spinel structure with Fe^{3+} at tetrahedral 8*a* positions and a 1:3 mixture of Li^+ and Fe^{3+} at octahedral positions. The latter are 16*d* Wyckoff's positions for disordered (*Fd*3*m*) form, and 4*b*+12*d* for the ordered ($P4_132/P4_332$) form [1].

Although the distribution of lithium ions in both cationic spinel sublattices could be expected in the mixed, normal and inverse, spinel solid solutions, the results reported are divergent. In the single phase $(1-x)Li_{0.5}Fe_{2.5}O_4 \cdot xMnFe_2O_4$ solid solutions, all lithium ions were found in octahedral sites [2]. On the other hand, $Li_{0.5}Mn_xFe_{2.5-x}O_4$ became tetragonally distorted when $x \geq 1.75$, and for $x=0.5$ the tetrahedral positions for all Li^+ ions have been established [3]. It is striking that in both experiments, the lithium deficiency appears, caused by the increase of manganese content. Distribution of Li^+ ions in tetrahedral, as well as in octahedral sites has been reported for the $LiMnFeO_4$ spinel, prepared by solid state reaction methods [4], and by a coprecipitation method followed by thermal crystallization [5]. Cation distribution over a spinel lattice of the whole $(1-x)LiMn_2O_4 \cdot xLi_{0.5}Fe_{2.5}O_4$ solid solution series has been determined recently by conventional techniques using structure factors obtained from the single, integrated X-ray powder reflection intensities [6]. We have now undertaken a detailed study on the lithium

*Corresponding author.
E-mail address: emilia@main.amu.edu.pl (E. Wolska)

0925-8388/99/$ – see front matter
PII: S0925-8388(98)01007-X

ion distribution, and on the Fe:Mn ratio limits, causing the order–disorder transition, using the Rietveld structure refinement method. This work contributes to the comprehensive studies, inclusive of experimental and computational techniques, on the modelling of defect structures and of the cation distribution in spinel oxide solid solutions [7].

2. Experimental details

Samples of solid solutions with compositions $(1-x)LiMn_2O_4 \cdot xLi_{0.5}Fe_{2.5}O_4$ were prepared from mixtures of iron–manganese oxide precursors with appropriate quantities of Li_2CO_3, by thermal treatment at 600–750°C in air. Precursors were prepared by autoclaving the amorphous Fe(III)Mn(II)-hydroxides coprecipitated from (Fe,Mn)-nitrates with LiOH, at 150°C (4.76×10^5 Pa) for 4 days.

X-ray diffraction studies were performed with a computerised TUR-61 (HZG-3) diffractometer employing the Mn-filtered Fe Kα radiation. The structural refinements were performed using the Rietveld program package GSAS [8,9]. Data from 18° to 90° (2θ) with resolution of 0.04° (2θ) were included into calculations.

Infrared absorption spectra were registered on 'Perkin-Elmer-180' spectrophotometer, using CsI pellets.

3. Results and discussion

The structure of Mn–Fe oxide precursors changed successively, with the increase of Fe/(Fe+Mn) molar ratio, from the tetragonal hausmannite (Mn_3O_4), throughout the cubic spinel ($MnFe_2O_4$), to hexagonal hematite (α-Fe_2O_3). The samples consisted of the respective compounds or their mixtures [10–12]. After heating in air at 750°C with Li_2CO_3, however, the single crystalline samples were formed, displaying exclusively spinel structure. Examples of solid state reactions for different precursors may be written:

$$Mn^{II}Mn_2^{III}O_4 + 3\,Li_2CO_3 + 5/2\,O_2 \rightarrow 6\,LiMn^{III}Mn^{IV}O_4 + 3\,CO_2 \quad (1)$$

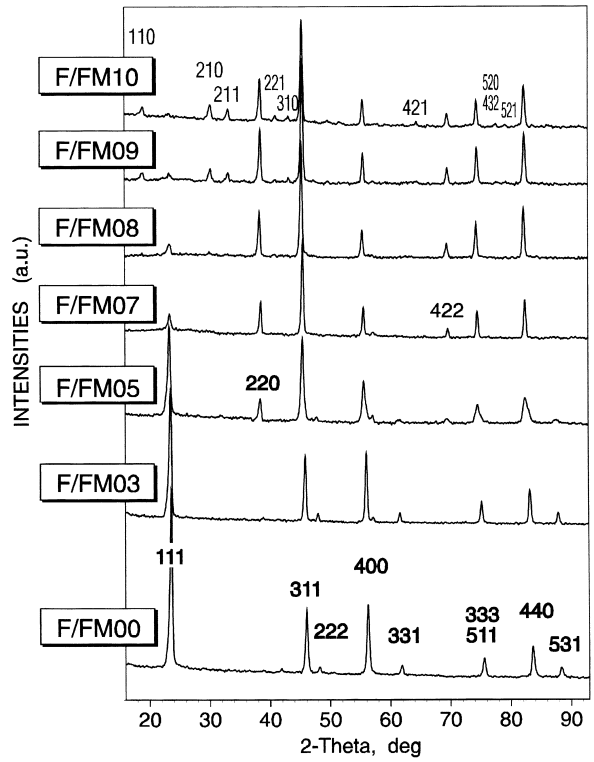

Fig. 1. X-ray powder diffraction patterns of lithium–iron–manganese spinel-type oxides. (Fe Kα radiation.) Symbols correspond to samples described in Table 1.

$$Mn^{II}Mn_2^{III}O_4 + 3\,Mn^{II}Fe_2^{III}O_4 + 3\,Li_2CO_3 + 5/2\,O_2 \rightarrow 6\,LiFe^{III}Mn^{IV}O_4 + 3\,CO_2 \quad (2)$$

$$3\,Mn^{II}Fe^{III}O_4 + 3/2\,Li_2CO_3 + 5/4\,O_2 \rightarrow 4\,Li_{0.75}Fe_{1.5}^{III}Mn_{0.25}^{III}Mn_{0.5}^{IV}O_4 \quad (3)$$

$$5\,Fe_2^{III}O_3 + Li_2CO_3 \rightarrow 2\,LiFe_5^{III}O_8 + CO_2. \quad (4)$$

Composition details of solid solutions $(1-x)LiMn_2O_4 \cdot xLi_{0.5}Fe_{2.5}O_4$, obtained from precursors with Fe/(Fe+Mn) molar ratio increasing from 0 to 1, are collected in Table 1.

The X-ray powder diffraction patterns of these samples, presented in Fig. 1, reveal the main reflections characteristic of the spinel-type structure. A decrease of the intensity ratio of $I111)/I(311)$ lines indicates the removal of lithium ions from tetrahedral to octahedral sites, i.e. the trans-

Table 1
Compositions and cation distribution in the solid solution series of $Li_{1-0.5x}Fe_{2.5x}Mn_{2-2x}O_4$

Symbol of sample	Fe/(Fe+Mn) molar ratio	x in $Li_{1-0.5x}Fe_{2.5x}Mn_{2-2x}O_4$	Stoichiometric Li content	Total Li introduced as Li_2CO_3
F/FM00	0.0	0.000	1.0000	1.00
F/FM03	0.3	0.255	0.8724	0.90
F/FM05	0.5	0.444	0.7778	0.80
F/FM07	0.7	0.651	0.6744	0.70
F/FM08	0.8	0.762	0.6190	0.65
F/FM09	0.9	0.878	0.5610	0.60
F/FM10	1.0	1.000	0.5000	0.50

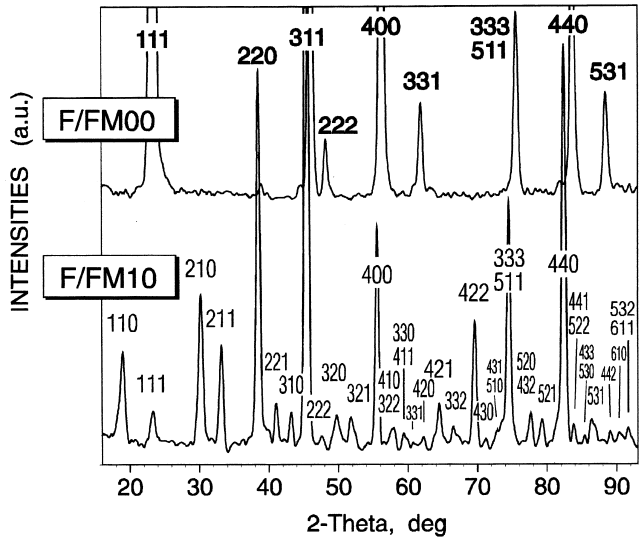

Fig. 2. X-ray powder diffraction pattern of lithium ferrite, $LiFe_5O_8$, showing the 'superstructure' reflections of ordered spinel (space group $P4_132/P4_332$), compared to $LiMn_2O_4$ (space group $Fd3m$).

formation of a normal spinel ($LiMn_2O_4$) into an inverse spinel ($LiFe_5O_8$), with the increase of Fe^{3+} content. The appearance of additional reflections (110, 210, 211, 221, . . .) on the X-ray patterns of samples F/FM08–F/FM10 shows a tendency to the 1:3 ordering of cations in octahedral positions, resulting in the reduction of the crystal symmetry from an $Fd3m$ to $P4_132$ ($P4_332$) space group, when the Fe/(Fe+Mn) molar ratio exceeds 0.7. The X-ray pattern of a typical ordered inverse spinel, $Fe[Li_{0.5}Fe_{1.5}]O_4$ (sample F/FM10) has been compared to the normal spinel, $Li[Mn_2]O_4$ (sample F/FM00), in Fig. 2.

For the Rietveld profile analysis of $Li_{1-0.5x}Fe_{2.5x}Mn_{2-2x}O_4$ series, the data obtained for a similar solid solution series from measurements of integrated intensities of single X-ray lines have been used as starting parameters [6,11]. The X-ray patterns have been classified into two different sets. The first set consists of samples with $0 \leq Fe/(Fe+Mn) \leq 0.7$ ($0 \leq x \leq 0.65$), for which all reflections can be indexed according to the space group $Fd3m$. The X-ray patterns of the second set ($0.7 \leq Fe/(Fe+Mn) \leq 1.0$) are characterised by additional reflections and can be assigned to the space group $P4_132$ ($P4_332$). Structural and cell parameters from the Rietveld profile refinement of both sets of X-ray patterns are presented in Tables 2 and 3, respectively. For sample F/FM07 ($x=0.65$), with X-ray pattern showing the first symptoms of the cation ordering, the refinement has been carried out assuming both the face centred cubic and the cubic primitive type of unit cell. Observed, calculated and difference profiles, resulting from the Rietveld analysis of powder X-ray diffraction data, for the end-members of the solid solution series, $LiMn_2O_4$ and $Li_{0.5}Fe_{2.5}O_4$, are presented in Figs. 3 and 4, respectively.

The occupancy of manganese in the 16*d* (B) sites, 0.82 in sample F/FM00, is in good agreement with the arrangement $Li[Li_{0.33}Mn_{1.67}]O_4$, in which 0.33 Li^+ ions compensate the oxidation of Mn^{3+} to Mn^{4+} [13]. The increase of Fe^{3+} content in samples appears to be associated with a decrease of total lithium content and with a simultaneous migration of Li^+ from tetrahedral into octahedral sites. The preference of Li^+ to occupy the Wyckoff's 4*b* positions is strongly marked only in samples F/FM09 and F/FM10 (see 'occupancies' in Table 3), although the X-ray reflections characteristic for the cubic primitive unit cell appear already for lower Fe/(Fe+Mn) ratios, e.g. for sample F/FM08.

Changes in the interatomic distances in the AB_2O_4 spinel lattice, determined by Rietveld analysis (Table 4) are in good agreement with the increase of lattice constants and with the decrease in the values of the oxygen *u* parameter.

The infrared spectrum may be of great importance in resolving the problem of order/disorder in the spinel structure. Group theory predicts, based on the factor group approximation, that in a cubic spinel, with the space group $Fd3m$, four infrared active vibrations should be present. For a normal-inverse disorder, there is no change in space group, and therefore both normal and inverse spinel are

Table 2
Structural parameters for $(1-x)LiMn_2O_4 \cdot xLi_{0.5}Fe_{2.5}O_4$, with $0 \leq x \leq 0.65$, from the Rietveld refinement in $Fd3m$ space group

Atom	Site	Coordinates			Occupancy determined for sample			
		x	*y*	*z*	F/FM00	F/FM03	F/FM05	F/FM07
Li(1)	8*a*	0	0	0	1.00(9)	0.950(4)	0.578(3)	0.275(3)
Fe(1)	8*a*	0	0	0	–	0.050(8)	0.415(6)	0.725(6)
Li(2)	16*d*	0.625	0.625	0.625	0.203(18)	0.025(2)	0.064(2)	0.226(1)
Fe(2)	16*d*	0.625	0.625	0.625	–	0.275(4)	0.365(3)	0.433(3)
Mn3(1)	16*d*	0.625	0.625	0.625	0.398(9)	0.200	0.368	0.1138
Mn4(1)	16*d*	0.625	0.625	0.625	0.398(9)	0.500	0.206	0.2275
a(Å)					8.2164(4)	8.24888(25)	8.3091(4)	8.30589(22)
u					0.3883(4)	0.3880(5)	0.3927(5)	0.3865(5)
R_{wp}					7.18%	5.91%	4.85%	4.57%
R_p					5.20%	4.12%	3.58%	3.55%
B_{iso}	($B_{Li}=B_{Mn}=B_{Fe}=B_O$)			1.97 Å^2				

Table 3
Structural parameters for $(1-x)LiMn_2O_4 \cdot xLi_{0.5}Fe_{2.5}O_4$, with $0.65 \leq x \leq 1.0$, from the Rietveld refinement in $P4_132/P4_332$ space group

Atom	Site	Coordinates			Occupancy determined for sample			
		x	*y*	*z*	F/FM07	F/FM08	F/FM09	F/FM10
Li(1)	4*b*	0.625	0.625	0.625	0.222(9)	0.270(10)	0.996(4)	0.73(14)
Fe(1)	4*b*	0.625	0.625	0.625	0.435(5)	0.508(5)	0.040(4)	–
Mn3(1)	4*b*	0.625	0.625	0.625	0.117(7)	0.060(7)	0.060(6)	–
Mn4(1)	4*b*	0.625	0.625	0.625	0.231(7)	0.138(7)	0.060(6)	–
Li(2)	12*d*	0.125	0.375	−0.125	0.172(1)	0.243(1)	–	–
Fe(2)	12*d*	0.125	0.375	−0.125	0.434(4)	0.1511(4)	0.840(1)	0.861(24)
Mn3(2)	12*d*	0.125	0.375	−0.125	0.113(2)	0.082(2)	0.034(2)	–
Mn4(2)	12*d*	0.125	0.375	−0.125	0.227(2)	0.160(2)	0.087(2)	–
Li(3)	8*c*	0	0	0	0.277(5)	0.152(5)	0.101(2)	–
Fe(3)	8*c*	0	0	0	0.723(5)	0.848(5)	0.917(2)	0.873(17)
a(Å)					8.30591(22)	8.32825(22)	8.31084(21)	8.31437(22)
u					0.3865(5)	0.3856(6)	0.3839(6)	0.3787(9)
R_{wp}					4.57%	4.20%	4.18%	4.01%
R_p					3.54%	3.11%	3.12%	3.09%
B_{iso}	$(B_{Li}=B_{Mn}=B_{Fe}=B_O)$			1.97 Å^2				

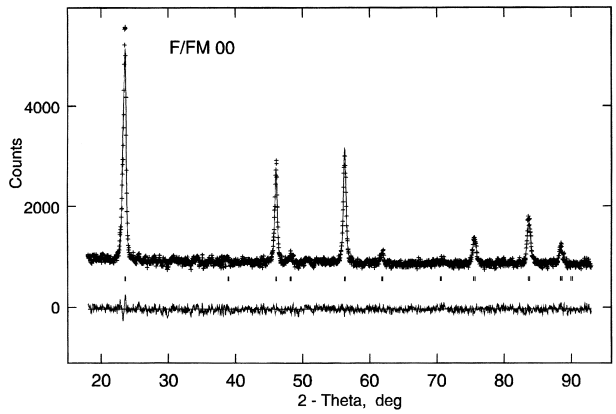

Fig. 3. Observed, calculated and difference profiles resulting from the Rietveld analysis of powder X-ray diffraction data collected on $LiMn_2O_4$ (space group *Fd*3*m*).

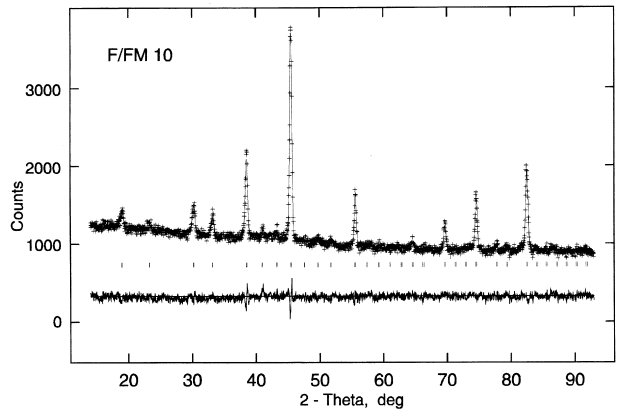

Fig. 4. Observed, calculated and difference profiles resulting from the Rietveld analysis of powder X-ray diffraction data collected on $LiFe_5O_8$ (space group $P4_132/P4_332$).

expected to have the same number of absorption bands. However, the number of active bands increases significantly with the lowering of crystal symmetry, caused by the tetragonal distortion or by the ordering of cations and/or vacancies [14,15]. Thus for tetragonal spinel the theory predicts 10, and for the ordering in octahedral sublattice 21 infrared active bands [16].

In general, the recorded spectra of $LiMn_2O_4$ show two intense bands between 400 and 700 cm^{-1} with two smaller sharper bands at lower frequencies (200–300 cm^{-1}), but the latter are sometimes difficult to record (Fig. 5). Incorporating iron in the spinel lattice first produced only minor changes in the mid-infrared (800–200 cm^{-1}) spectroscopic region. However, significant differences are

Table 4
Interatomic distances in the $(1-x)LiMn_2O_4 \cdot xLi_{0.5}Fe_{2.5}O_4$ spinel solid solutions

Bond	Space group *Fd*3*m* Bond length (Å)				Space group $P4_332$ Bond length (Å)			
	F/FM00	F/FM03	F/FM05	F/FM07	F/FM07(a)	F/FM08	F/FM09	F/FM10
Fe,Li(A)–Fe,Li,Mn(B)	3.4056(10)	3.41980(9)	3.44475(17)	3.44344(8)	3.44344(8)	3.45271(8)	3.44549(7)	–
Fe,Li(A)–O	1.978(6)	1.972(8)	2.054(7)	1.964(8)	1.964(8)	1.955(8)	1.928(9)	1.832(14)
Fe,Li,Mn(B)–Fe,Li,Mn(B)	2.9043(7)	2.91642(9)	2.93770(16)	2.93658(8)	2.93658(5)	2.94448(6)	2.93833(5)	2.9439(26)
Fe,Li,Mn(B)–O	1.9452(33)	1.960(4)	1.9415(35)	1.986(4)	1.986(4)	1.998(4)	2.006(5)	2.065(8)

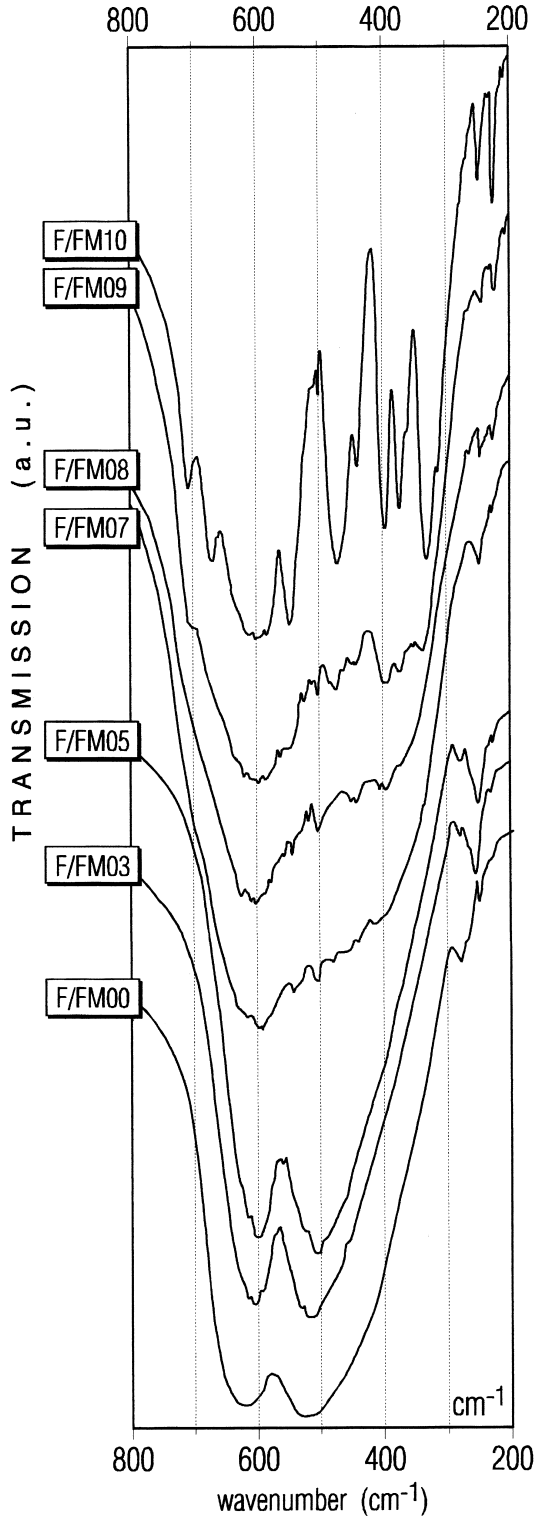

Fig. 5. Infrared spectra in the lattice vibration region of a series of solid solutions of $Li_{1-0.5x}Fe_{2.5x}Mn_{2-2x}O_4$. Symbols of samples as in Table 1.

observed with the increase of the Fe/(Fe+Mn) ratio, associated with increasing tendency of lithium ions to move from tetrahedral into octahedral sublattice. The multiplication of absorption bands, observed for Fe/(Fe+Mn)≥0.7, provides evidence for the reduction of crystal symmetry caused by the ordering of Li^+ in the 4*b* Wyckoff's positions of the cubic primitive unit cell ($P4_132/P4_332$ space group).

4. Conclusions

Single phase spinel compounds have been obtained for the solid solution series, $(1-x)LiMn_2O_4 \cdot xLi_{0.5}Fe_{2.5}O_4$, in the whole range of *x*, irrespective of structure of the iron–manganese oxide precursors. The distribution of lithium ions over the tetrahedral (A) and octahedral (B) positions of spinel (AB_2O_4) lattice has been established. The preference of Li^+ ions to occupy first the B sites of spinel lattice and then to order in the 'lithium positions' of a cubic primitive cell, related with the reduction of crystal symmetry, increases with *x*, i.e. with the increase of Fe/(Fe+Mn) molar ratio in samples.

Acknowledgements

The authors would like to thank the British–Polish Joint Research Collaboration Programme (project no. WAR/992/123) for partial support of this research.

References

[1] P. Braun, Nature (London) 170 (1952) 1123.
[2] F. Petit, M. Lenglet, Solid State Commun. 86 (1993) 67.
[3] E. Polert, Progr. Crystal Growth Charact. 9 (1984) 263.
[4] G. Blasse, Philips Res. Rep. 20 (1965) 528.
[5] Y.F. Liu, Q. Feng, K. Ooi, J. Colloid Interface Sci. 163 (1994) 130.
[6] E. Wolska, K. Stempin, O. Krasnowska-Hobbs, Solid State Ionics 101–103 (1997) 527.
[7] C.R.A. Catlow, R.G. Bell, J.D. Gale, J. Mater. Chem. 4 (1994) 781.
[8] A.C. Larsen and R.B. Von Dreele, Los Alamos Labor. Rep., NO-LA-U-86-748 (1987).
[9] R.A. Young (Ed.), The Rietveld Method, Oxford University Press, 1993.
[10] J. Kaczmarek, E. Wolska, Solid State Ionics 63–65 (1993) 633.
[11] W. Wolski, J. Kaczmarek, J. Magn. Magn. Mater. 136 (1983) 190.
[12] E. Wolska, K. Stempin, Mater. Sci. Forum 278–281 (1998) 618.
[13] T. Tokada, E. Akiba, F. Izumi, B.C. Chakoumakos, J. Solid State Chem. 130 (1997) 74.
[14] W.B. White, B.A. DeAngelis, Spectrochim. Acta 23A (1967) 985.
[15] G.C. Allen, M. Paul, Appl. Spectrosc. 49 (1995) 451.
[16] J. Preudhomme, Ann. Chim. 9 (1974) 31.